European Journal of Medicinal Chemistry Reports 16 (2026) 100327

Contents lists available at ScienceDirect

European Journal of Medicinal Chemistry Reports

journal homepage: www.editorialmanager.com/ejmcr/default.aspx

Fragment-based discovery of novel small molecule targeting *human* BAG3

Annagiulia Favaro [a], Chiara Marchioro [b,c], Martina Canton [b,c], Thomas Stella [a], Romeo Romagnoli [d], Elena Mariotto [b,c,*,1], Mattia Sturlese [a,**,1], Giampietro Viola [b,c,***,1]

[a] Molecular Modeling Section (MMS), Department of Pharmaceutical and Pharmacological Sciences, University of Padova, via Marzolo 5, 35131, adova, Italy
[b] Laboratory of Pediatric Hematology-Oncology Department of Women's and Children's Health, University of Padova, Via Giustiniani 3, 35128, Padova, Italy
[c] Istituto di Ricerca Pediatrica (IRP), Corso Stati Uniti 4F, 35127, Padova, Italy
[d] Department of Chemical, Pharmaceutical and Agricultural Sciences, University of Ferrara, 44121, Ferrara, Italy

ARTICLE INFO

Keywords:
Fragment-based drug discovery (FBDD)
BAG3 protein
Protein–protein interactions (PPIs)
Intrinsically disordered proteins (IDPs)
Small-molecule inhibitors

ABSTRACT

Bcl-2-associated athanogene 3 (BAG3) is a multifunctional co-chaperone protein that regulates apoptosis, autophagy, and proteostasis through interactions with HSP70 and other partners. Overexpression of BAG3 contributes to tumor cell survival, metastasis, and chemotherapy resistance, making it an appealing but challenging anticancer target due to its intrinsic disorder and lack of structural data. Here, we report a fragment-based drug discovery (FBDD) approach to identify novel small molecules targeting *human* BAG3. A fragment library of 783 compounds was screened using a thermal shift assay (TSA) against recombinant BAG3 expressed in mammalian cells, followed by hit validation through ligand-observed NMR (WaterLOGSY). Eleven fragments stabilized the protein, and seven were confirmed as binders. Among them, a 6-chloro-2-oxindole fragment (**Fr1**) exhibited the strongest interaction, with a dissociation constant (K_D) of 97.8 ± 11.1 μM. Structure–activity relationship (SAR) studies focused on maintaining the 6-chloro-2-oxindole core and optimizing substitutions at position 3, identified derivative **7** as a promising lead. Derivative **7** bound BAG3 with improved affinity ($K_D \approx 22$ μM), as confirmed by grating-coupled interferometry, and displaced **Fr1** in competition NMR assays. This work demonstrates the feasibility of applying FBDD to intrinsically disordered and structurally unresolved proteins such as BAG3, providing a validated chemical starting point for the development of selective BAG3 inhibitors. These findings expand the druggability landscape of BAG3 and highlight fragment-based methodologies as powerful tools to explore protein–protein interaction targets previously considered intractable.

1. Introduction

The Bcl-2-associated athanogene 3 (BAG3) is a 75 kDa cytosolic protein composed of 575 amino acids, belonging to the BAG family [1]. This family primarily regulates protein homeostasis, acting as co-chaperones for heat shock protein 70 (HSP70), modulating its activity and association with client proteins [2,3]. BAG3, in particular, is a multifaceted protein involved in various biological processes, including apoptosis [4–10], autophagy [11–14], stress response, and cell movement, all supporting cellular homeostasis [15]. It is ubiquitously expressed in all tissues, but is particularly abundant in the heart and skeletal muscles [16].

In cancer, BAG3 overexpression contributes to tumor cell survival, metastasis, and chemotherapy resistance, primarily by suppressing apoptosis and promoting autophagy [12], [17–20]. Its dysregulation has been linked to both solid and hematologic malignancies [4,7,8,21,22], highlighting it as an attractive therapeutic target.

Structurally, BAG3 has two main domains, according to the protein family database (PFAM) [23], and several motifs mediating a plethora of protein–protein interactions (PPIs) [24] (Fig. S1A). At the N-terminus, a

* Corresponding author. Laboratory of Pediatric Hematology-Oncology Department of Women's and Children's Health, University of Padova, Via Giustiniani 3, 35128, Padova, Italy.
** Corresponding author.
*** Corresponding author. Laboratory of Pediatric Hematology-Oncology Department of Women's and Children's Health, University of Padova, Via Giustiniani 3, 35128, Padova, Italy.
E-mail addresses: elena.mariotto@unipd.it (E. Mariotto), mattia.sturlese@unipd.it (M. Sturlese), giampietro.viola.1@unipd.it (G. Viola).
[1] Equally contributing authors.

https://doi.org/10.1016/j.ejmcr.2026.100327
Received 14 November 2025; Received in revised form 1 February 2026; Accepted 5 February 2026
Available online 6 February 2026

WW domain mediates the interaction with proline-rich motifs of proteins involved in cell adhesion, cancer suppression, and tumorigenesis [19,25]. Two IPV and one proline-rich PXXP motifs then follow. They allow BAG3 to bind to small heat shock proteins B6 and B8 (HspB6, and HspB8) [25,26] and to dynein, respectively [27]. Between the two IPV motifs, an RSQS sequence enables the interaction with 14-3-3 proteins [28]. At the C-terminus is the BAG domain. It consists of 77 amino acids and binds to the ATPase binding site of HSP70, allowing BAG3 to act as a co-chaperone, and to the antiapoptotic protein Bcl-2 [3]. Despite increasing insights into the biological functions of *human* BAG3, its three-dimensional (3D) structure remains unresolved. To date, structural data are limited to the BAG domains of the *murine* (PDB ID: 1UK5) and *Arabidopsis thaliana* (PDB ID: 4HWF) orthologs, both of which adopt a fold comprising three short parallel α-helices [29,30] (Fig. S1A). The main challenge in obtaining an experimental structure of *human* BAG3 lies in its high conformational flexibility (Fig. S1B). In support of this, AlphaFold predictions indicate that BAG3 is predominantly intrinsically disordered (AlphaFold Entry: 095817).

Undoubtedly, a more detailed picture of the 3D structure of *human* BAG3 would improve the development of BAG3 inhibitors. Early attempts to inhibit this protein relied on HSP70 allosteric inhibitors (e.g., MKT-077 [31], YM-08 [32], and JG98 [33]) that bind near the nucleotide-binding domain of HSP70 in the ADP-bound state, thereby disrupting the HSP70–BAG interaction; however, their therapeutic potential is limited by photoreactivity and poor solubility. A structure-based virtual screening in 2018 identified compound 28, a 2, 4-thiazolidinedione derivative, as the first small molecule reported to bind the BAG domain of human BAG3 and inhibit the BAG3–HSP70 interaction [34]. Binding affinities ranged from nanomolar (bacterial expression) to high micromolar (mammalian expression). Subsequent scaffold optimization yielded compounds **6** and **FB49**, which showed improved affinity for full-length BAG3 and antiproliferative activity in cancer cell lines [14,35]. Despite these efforts, human BAG3 remains an undrugged target, with no selective, high-affinity small-molecule inhibitors available. A summary of reported BAG3 or BAG3–HSP70 modulators is provided in Table S1.

In this work, we describe a fragment-based drug discovery (FBDD) approach as an effective strategy to identify novel small molecules targeting *human* BAG3. FBDD is particularly suited to address targets such as intrinsically disordered proteins (IDPs) and PPI interfaces, historically considered "undruggable," as fragments, with their low chemical complexity, can efficiently explore chemical space and bind to key interaction hotspots often inaccessible to larger molecules [36–42]. We screened an in-house fragment library [43] against *human* BAG3 produced in mammalian cells, using a combination of orthogonal biophysical techniques tailored for high molecular weight proteins with low production yields. The use of mammalian expression systems was chosen to preserve post-translational modifications, which are crucial from both structural and functional perspectives [18,22,28]. These modifications may significantly influence the disorder propensity of *human* BAG3. Thermal shift assay (TSA) was employed for initial screening, followed by ligand-observed (LO) nuclear magnetic resonance (NMR) for hit validation. This identified a 6-chloro-2-oxindole--based fragment, **Fr1**, as the most promising hit. Preliminary structure–activity relationship (SAR) studies, including catalogue exploration and synthesis of novel analogues, allowed the optimization of **Fr1** into derivative **7**, which showed improved binding affinity.

2. Results and discussion

2.1. Fragment-based primary screening by thermal shift assay: identification of eleven fragments as potential hits

A total of 783 fragments from our in-house fragment library [43] were initially screened against *human* BAG3-His using TSA, which proved well-suited for this system due to its speed and low protein consumption. A large number of the fragments destabilized the protein, inducing a negative thermal shift of up to five degrees below the average melting temperature (Tm) of human BAG3 (45.7 °C; see Fig. S2). On the contrary, a subset of fragments stabilized the protein, resulting in a positive ΔTm ranging from 0.1 to 9.6 °C.

Only fragments that induced a positive shift in the melting temperature of the protein were considered. Specifically, fragments determining a ΔTm greater than +1 °C relative to the average melting temperature of the free protein (Tm = 45.7 °C, based on three replicates). Based on this criterion, twenty-six fragments were selected for further analysis and subsequently reassessed in three independent experiments to confirm the reproducibility of the observed thermal shifts. Fragments that consistently produced a positive ΔTm exceeding twice the standard deviation (2 SD) of the apo-protein melting temperature were classified as potential hits. Based on this criterion, eleven of the twenty-six fragments were advanced to the NMR validation (Table 1, Fig. S3).

Fragment **Fr4** induced a substantial thermal stabilization of BAG3, with a ΔTm of 9.6 °C (Table 1, Fig. S3D), an unusually high shift for a fragment-sized molecule. Interestingly, **Fr2** and **Fr3** share high chemical similarity with **Fr4**, each featuring two phenyl rings connected by different linkers—methylene (**Fr2**), oxygen (**Fr3**), and an anilinic nitrogen (**Fr4**)—and bearing a primary amino group in distinct positions on one of the aromatic rings. Despite these similarities, the three compounds showed different ΔTm values (Table 1, Fig. S3B–D), suggesting that both the chemical nature of the linker and the position of the amino group influence the binding to the protein. In particular, the presence of an anilinic NH linker in **Fr4**, capable of acting as both a hydrogen bond donor and acceptor, combined with an ortho-positioned amino group, appears to contribute to the pronounced thermal stabilization observed.

2.2. Hits validation and prioritization by NMR spectroscopy

Fragments identified as potential hits in the TSA primary screen (Table 1) were further validated by ligand-observed NMR spectroscopy using the WaterLOGSY experiment. This technique is particularly well suited for fragment-based screening, as it enables the direct detection of weak protein–ligand interactions and provides an unambiguous criterion for binding based on magnetization transfer from the protein to the ligand.

Each of the eleven fragments was analyzed by WaterLOGSY in the absence and presence of human BAG3-His. In the presence of the protein, seven fragments (Fr1–Fr4 and Fr6–Fr8) displayed a clear inversion of signal phase, adopting the same NOE sign as the protein. This behavior is diagnostic of ligand binding and reflects the transfer of protein magnetization to the ligand through intermolecular NOE effects. In contrast, the remaining four fragments did not show any signal inversion upon protein addition and were therefore classified as non-

Table 1
Overview of TSA data for the eleven fragments selected as potential hits.

ID	Tm[a](°C)	ΔTm (°C)
human BAG3-His	45.7 ± 0.1	0
Fr1	47.5 ± 0.2	1.8
Fr2	47.6 ± 0.7	1.9
Fr3	48.1 ± 0.9	2.4
Fr4	55.3 ± 0.3	9.6
Fr5	47.8 ± 0.2	2.1
Fr6	47.7 ± 0.1	2
Fr7	49.2 ± 0.0	3.5
Fr8	47.1 ± 0.5	1.4
Fr9	46.4 ± 0.4	0.7
Fr10	47.2 ± 0.3	1.5
Fr11	48.4 ± 0.1	2.7

[a] The melting temperature of each sample was calculated by JTSA software (Bond, PS. JTSA. http://paulsbond.co.uk/jtsa), as described in Materials and Methods. Data are represented as mean ± SD.

binders. Based on this criterion, seven fragments were confirmed as bona fide BAG3 binders, corresponding to an overall hit rate of approximately 1%.

Beyond qualitative hit confirmation, WaterLOGSY experiments were also exploited to prioritize the validated fragments. For each ligand, a WaterLogsy (WLOGSY) factor was calculated for the protons most protected by the protein, providing a semi-quantitative measure of magnetization transfer efficiency and, indirectly, of binding strength under the experimental conditions. Higher WLOGSY factor values often indicate a larger fraction of ligand in the bound state at a fixed concentration and were therefore used to prioritize fragments for further characterization. As shown in Fig. 1A, the highest WLOGSY factor value (WLOGSY factor = 25.3) is observed for **Fr1**. This is followed by **Fr3** and **Fr2**, with comparable values (22.3 and 21.2, respectively). These findings are in good agreement with TSA data (Table 1), where **Fr3** showed a higher protein thermal stabilization (ΔTm = 2.4 °C) than **Fr2** (ΔTm = 1.8 °C).

Surprisingly, **Fr4**, despite its close structural similarity to **Fr2** and **Fr3**, displays a notably lower WaterLOGSY factor, suggesting that the presence of a hydrogen bond donor within the linker between the two aromatic rings may negatively affect the binding to the protein. This observation contradicts TSA results, where **Fr4** induced the most pronounced thermal stabilization (ΔTm = 9.6 °C, Table 1). Such a discrepancy between biophysical techniques might arise from **Fr4** engaging in multi-site interactions that globally stabilize the folded state of the protein (detected by TSA), but do not result in a specific binding interaction that would lead to greater magnetization transfer in the WaterLOGSY experiment.

2.3. Fr1 binding affinity estimation by WaterLOGSY experiments

To further characterize the binding of the top-ranking fragment **Fr1** to *human* BAG3-His, a five-point WaterLOGSY titration was performed to estimate its dissociation constant (K_D). The K_D for **Fr1** was determined to be 97.8 ± 11.1 μM (Fig. 1B and C). Remarkably, despite its small size, **Fr1** exhibits affinity comparable to that of first-generation mature compounds tested against *human* BAG3 produced in mammalian cells. For example, compound **28**—the first molecule reported to modulate the

A

ID	WaterLOGSY factor
Fr1	25.3
Fr3	22.3
Fr2	21.2
Fr6	20.9
Fr4	16.5
Fr7	10.8
Fr8	5.7

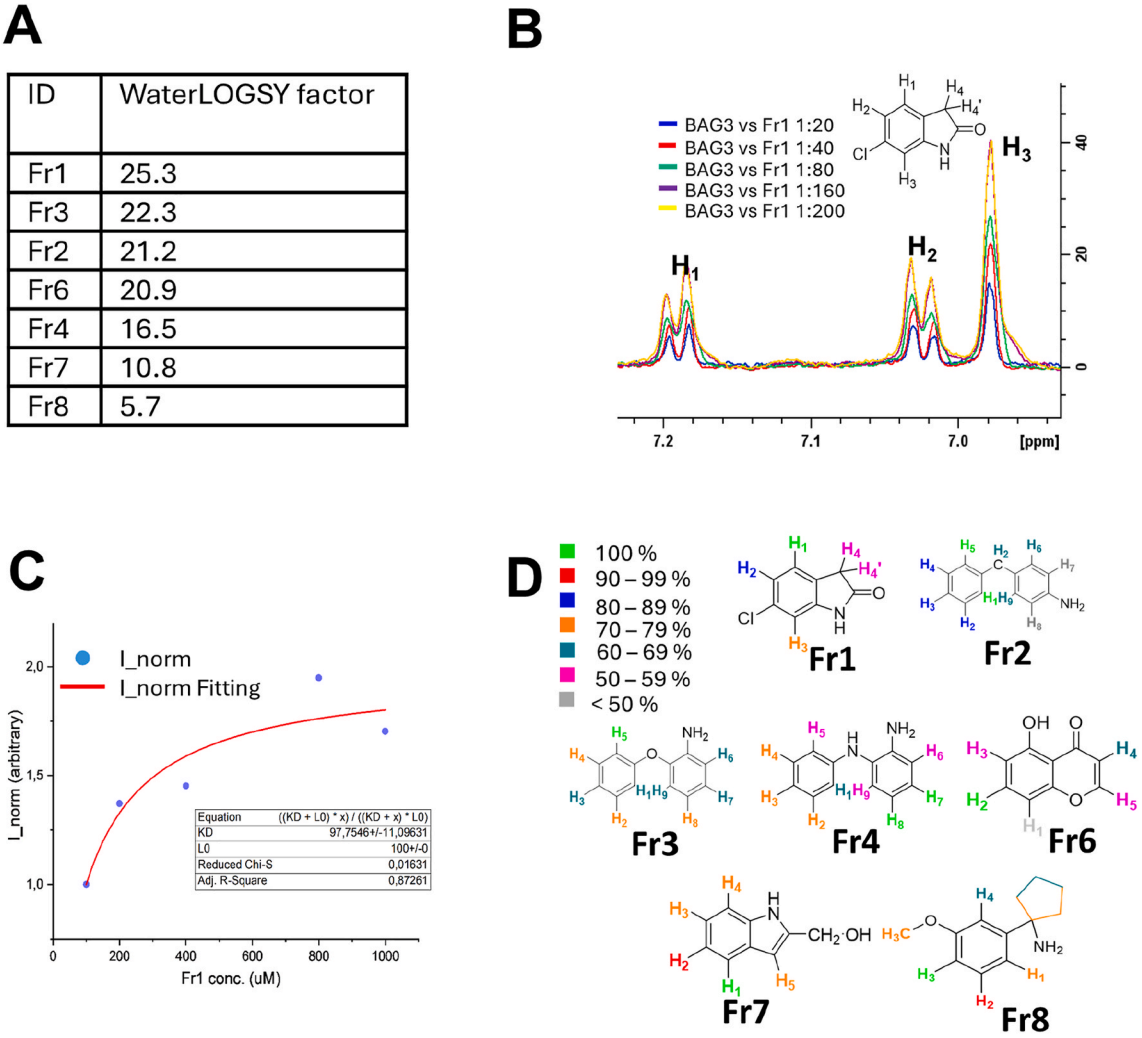

Fig. 1. Biophysical characterization by NMR of the binding of the seven fragments validated as *human* BAG3-His binders. (**A**) Overview of the WaterLOGSY factor-based ranking. (**B**) Superposition of WaterLOGSY spectra in the presence of *human* BAG3-His (5 μM) at increasing **Fr1** concentrations (from 200 μM to 1 mM). The spectra were recorded at 298 K on a 600 MHz spectrometer equipped with a nitrogen-cooled cryoprobe in 50 mM phosphate and 150 mM NaCl at pH 7.8. The spectra are phased, processed to display binders with an inverted phase relative to free ligands. (**C**) K_D estimation of **Fr1** through a five-point WaterLOGSY titration of the protein. The WaterLogsy (LOGSY) effect was normalized (I_norm) to 1 for the ligand concentration L0 and used as a reference to calculate relative LOGSY effects at different concentrations. The experimental data were fitted using equation (3) in Materials and Methods. (**D**) Graphical representation of epitope mapping for the seven fragment hits. Proton colors denote their degree of solvent exposure based on the WaterLOGSY effect: green protons are more protected by the protein, whereas gray protons are more exposed to the solvent.

BAG3 domain—and the optimized compound **FB49** have binding affinities of 233 ± 58 μM and 45 ± 6 μM, respectively [14]. Although these differences are modest in energetic terms, the approximately 98 μM K_D of **Fr1**, a non-drug-sized molecule, suggests greater binding efficiency relative to these larger compounds.

2.4. Elucidation of fragments binding epitopes via WaterLOGSY effect

A preliminary binding epitope mapping (Fig. 1D) of hit fragments was derived from WaterLOGSY data [44], enabled us to identify the proton atoms mainly involved in magnetization transfer and, hence, most likely in protein engagement.

For fragment **Fr1**, the largest WaterLOGSY effects (ranging from 70 to 100%) are observed for the protons of the benzene group, while protons H4 and H4′ show the smallest WaterLOGSY effect. This suggests that the benzene portion of 6-chloro-2-oxoindole is oriented toward the protein, while the 2-pyrrolidone fragment remains more solvent-exposed upon binding. A comparable binding epitope emerges for **Fr2** and **Fr3**: the unsubstituted benzylic group appears to be more protected by the protein from bulk water (WaterLOGSY effect in the range of 80-100% for **Fr2** and 65-100% for **Fr3**) compared to the anilinic group (WaterLOGSY effect <68% for **Fr2** and <74% for **Fr3**). Intriguingly, **Fr4**, which differs from **Fr3** only by the replacement of an oxygen atom with an amino group in the linker between the two aromatic rings, does not display a clear orientation at the binding site. The relatively high WaterLOGSY effects for most of its protons suggest that **Fr4** may adopt multiple binding modes. This observation supports the hypothesis that the previously noted discrepancy between TSA and NMR results for **Fr4** may originate from nonspecific interactions with the protein.

Epitope mapping of **Fr6** and **Fr7** indicates that the benzenic ring is more protected by *human* BAG3-His. Furthermore, while **Fr7** appears to adopt a defined binding orientation, **Fr6** may engage in multiple binding modes. As for **Fr8**, the protons at positions 6 and 5 exhibit the highest WaterLOGSY effects (>94%), whereas the rest of the molecule shows lower values (60–79%), suggesting greater solvent exposure.

2.5. Hit-to-lead optimization of Fr1

The absence of an experimentally resolved full-length structure of human BAG3, which contains several intrinsically disordered regions (Fig. S1B), prevents the application of structure-based drug design (SBDD) in the hit-to-lead process. Therefore, competition experiments were employed to assess whether fragment merging or fragment growing would be the most suitable strategy for optimizing **Fr1**. The fragment linking approach, which strongly relies on structural data, was not considered [36].

To evaluate the feasibility of fragment merging, we performed WaterLOGSY-based competition experiment to test whether two hits can bind BAG3-His simultaneously.

The most promising Fr1 was kept at a constant concentration, and the remaining six fragments were tested one at a time in combination with Fr1 for binding to BAG3-His. Observation of WaterLOGSY signal inversion for both ligands indicates binding to distinct, non-overlapping sites.

As shown in Fig. 2A, in the WaterLOGSY spectrum of Fr1 and Fr2 in the presence of BAG3-His, all signals from both ligands display the same

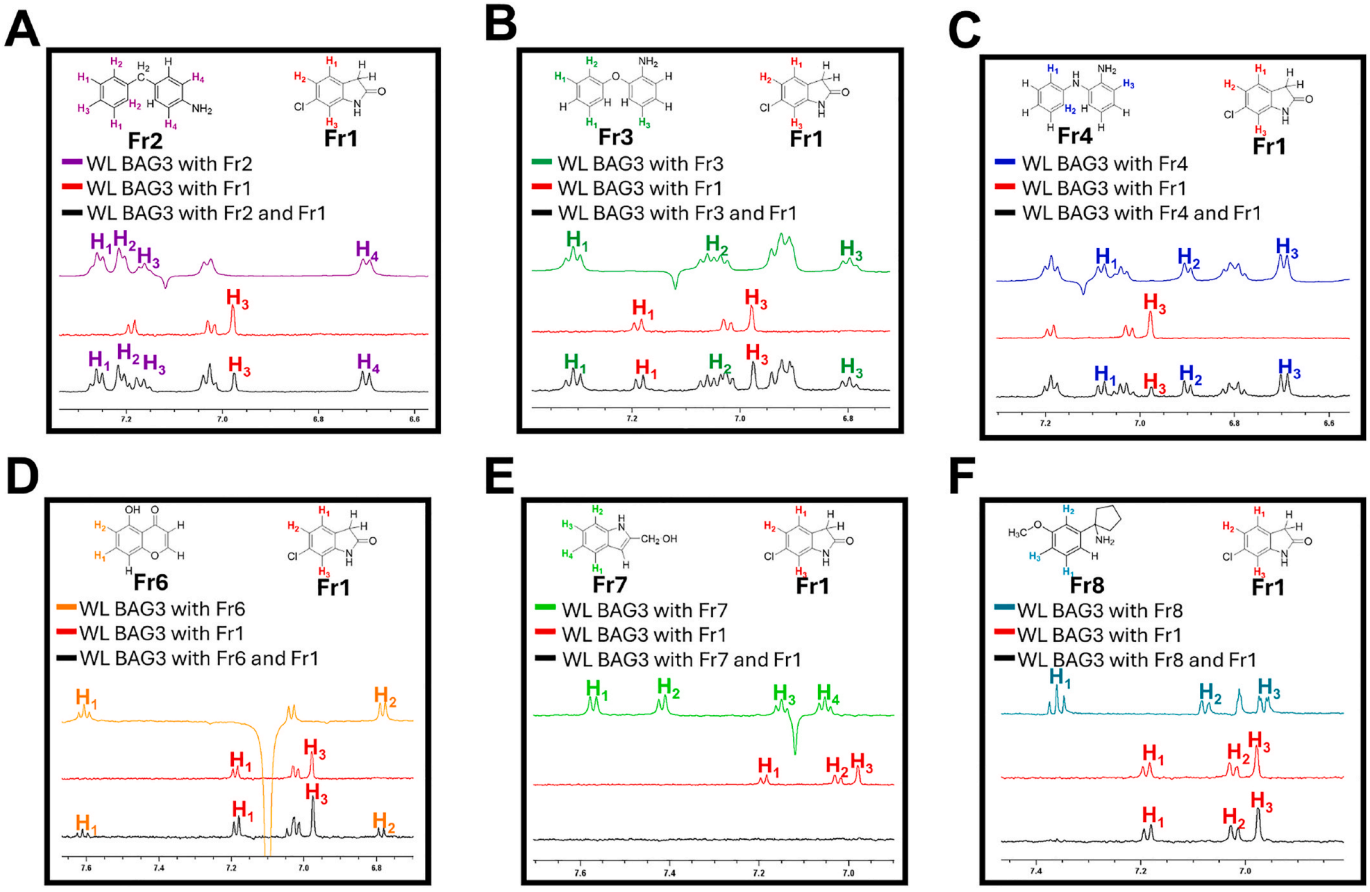

Fig. 2. Biophysical investigation of the simultaneous binding of two hits to *human* BAG3-His by LO NMR. Superposition of WaterLOGSY spectra of **Fr1** (in red), **Fr2** (**A**), **Fr3** (**B**), **Fr4** (**C**), **Fr6** (**D**), **Fr7** (**E**), and **Fr8** (**F**) alone or in combination with **Fr1** (in black) in the presence of 5 μM of BAG3 and with a ligand concentration of 100 μM. All spectra were acquired at 298 K on a Bruker 600 MHz spectrometer equipped with a nitrogen-cooled cryoprobe in 50 mM phosphate and 150 mM NaCl at pH 7.8. The spectra are processed, maintaining binders with a positive phase.

NOE sign as the protein, indicating their simultaneous binding to different sites on BAG3-His.

Similarly, fragments **Fr3**, **Fr4**, and **Fr6** remain binders in the presence of **Fr1** (Fig. 2B—D), evincing that they interact with different binding sites than **Fr1**.

In contrast, when **Fr7** is added to **Fr1**, no WaterLOGSY signals are observed either in the presence (Fig. 2E) or absence of the protein (data not shown), suggesting possible aggregation between **Fr1** and **Fr7** under these conditions. Notably, in the spectrum of **Fr1** and **Fr8** (Fig. 2F), only **Fr1** retains a detectable WaterLOGSY signal, while **Fr8** disappears. This indicates competitive binding at the same site, with **Fr1** likely having a greater affinity.

Overall, WaterLOGSY competition experiments suggest that **Fr1** and **Fr8** bind within the same region of BAG3-His and could, in theory, be merged into a larger molecule. However, the low chemical similarity between the two fragments does not support the identification of a shared scaffold that would facilitate a rational merging approach. Furthermore, in silico flexible alignment attempts (Fig. S5) did not provide a clear model for how these two fragments could be chemically combined.

2.6. Analogue synthesis and SAR studies on Fr1

To explore the potential for fragment growing, a structure–activity relationship (SAR) study was conducted on **Fr1** using a SAR by catalog approach [36]. Analogues were collected from three sources: (i) substructures of **Fr1** already screened in the in-house fragment library, (ii) commercially available compounds, and (iii) newly synthesized derivatives.

A common feature among nine previously tested fragments was the 2-oxindole scaffold (Fig. 3A), with **Fr1** being the only one carrying a chlorine atom at position 6. Both TSA and WaterLOGSY data confirmed that only **Fr1** binds to *human* BAG3-His, highlighting the essential role of the chlorine in position 6.

SAR studies thus focused on maintaining the 6-chloro-2-oxindole core, while exploring modifications at positions 3 and 1. According to epitope mapping (Fig. 2D), position 3 is the least engaged in binding, thereby representing a suitable site for fragment optimization without significantly affecting critical interactions or causing steric clashes.

2.7. Modification at position 3

A first set of analogues (derivatives **1**–**4**) consisted of 6-chloroisatin derivatives (Fig. 3B), all bearing a carbonyl group at position 3. These included one commercially available analog (**1**), and three N-alkylated derivatives (**2**–**4**), synthesized via N-alkylation of 6-chloroisatin with the appropriate alkyl bromide (ethyl 2-bromopropanoate, ethyl 3-bromopropanoate, and ethyl 2-bromoacetate, respectively) in the presence of sodium hydride in N,N-dimethylformamide (DMF) (Scheme 1).

WaterLOGSY experiments showed that none of the isatin derivatives bind to the protein, indicating that the carbonyl group at position 3 disrupts the interaction with *human* BAG3-His and should therefore be avoided in further optimization efforts.

To evaluate whether hydrophobic groups at position 3 could be beneficial, derivatives **5**, **6** (both commercially available), and **7** (Fig. 3B) were evaluated in WaterLOGSY experiments. Derivative **7** (as a racemic mixture) was prepared using an efficient, previously described, two-step approach, as reported in Scheme 2. This method involves a Knoevenagel condensation reaction of 6-chloro-2-oxindole with indole-3-carboxaldehyde in the presence of a catalytic amount of piperidine in refluxing ethanol, followed by the chemoselective reduction of the exocyclic double bond with $NaBH_4$ in ethanol at room temperature to yield derivative **7**.

WaterLOGSY experiments revealed that derivatives **5** and its desmethoxy analogue derivative **7** bind to the protein (Fig. 4A), indicating that hydrophobic substitutions at position 3 are well tolerated. Derivative **6** could not be evaluated due to precipitation in buffer at 100 μM, though its design remains relevant as it introduces π-conjugation at C3 without chirality.

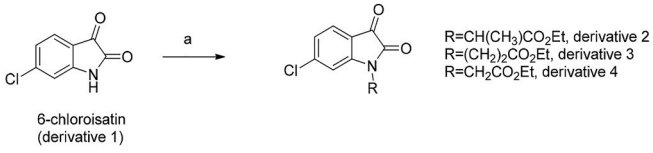

Scheme 1. Reagents: **a**: ethyl 2-bromopropanoate, ethyl 3-bromopropanoate, ethyl 2-bromoacetate (for the preparation of derivatives **2**–**4**, respectively), NaH, DMF, 0 °C to rt, 18 h.

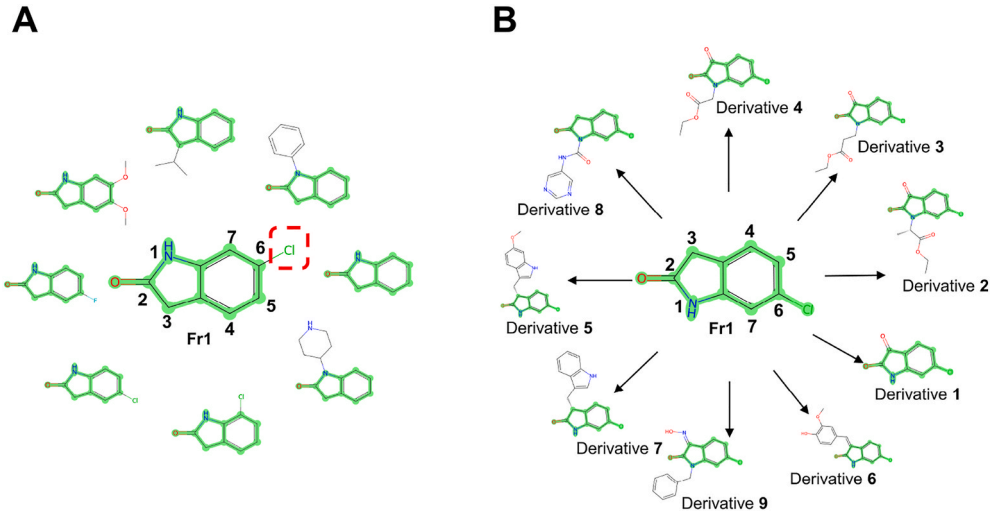

Fig. 3. SARs on the best-hit **Fr1**. (**A**) 2D structures of the nine 2-oxindoles resulted from a substructure search from the in-house fragment library and already screened against *human* BAG3-His. The 2-oxindole scaffold is highlighted in light green, while the chlorine atom at position 6 essential for binding to the protein is contoured in red. (**B**) 2D structures of the nine 6-chloro-2-oxindole molecules that were evaluated for fragment growing. The 6-chloro-2-oxindole scaffold is highlighted in light green.

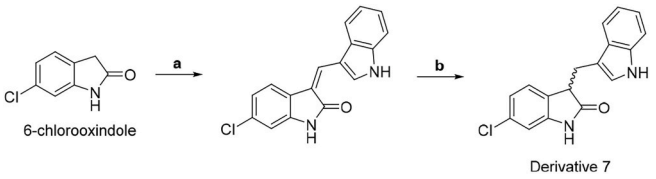

Scheme 2. Reagents: **a**: indole-3-carboxaldehyde, piperidine (cat.), EtOH, rx, 4h; **c**: $NaBH_4$, EtOH, 0 °C to rt.

2.8. Modification at position 1

To evaluate the effect of substitutions at position 1, derivative **8** (Fig. 3B), featuring a small N1 substituent, was purchased but excluded from binding studies due to poor solubility at 100 μM in buffer.

Derivative **9** (commercially available) (Fig. 3B), bearing modifications at both positions 1 and 3, was evaluated to explore potential synergistic effects. WaterLOGSY experiments showed binding to *human* BAG3-His, though with lower signal inversion compared to derivatives **5** and **7**, suggesting reduced affinity (Fig. 4A). Overall, the SAR indicates that hydrophobic substituents at position 3 are beneficial for binding, whereas N1 modifications are tolerated but do not appear to enhance affinity significantly.

Notably, derivative **7** produced the strongest signal inversion among the tested analogues, suggesting higher affinity. Grating-Coupled Interferometry (GCI) analysis confirmed this observation, yielding an estimated K_D of around 22 μM for compound **7** (Fig. 4B and S6A). Consistently, in a WaterLOGSY competition experiment, compound **7** was able to displace the original fragment **Fr1** (Fig. S6B), further confirming its higher affinity and binding at the same site. These results highlight the effectiveness of our **Fr1** optimization strategy, despite the challenges posed by the absence of an experimentally resolved target structure. The consistent improvement observed for substitutions at position 3 confirms this site as the most suitable vector for fragment growth. Moreover, the positive outcome with compound **7** suggests that hydrophobic substituents are well accommodated in this region, possibly interacting with apolar subpockets of the protein. Altogether, these findings provide a solid foundation for further optimization efforts focused on this vector.

3. Conclusions

This study presents the first fragment-based drug discovery (FBDD) campaign targeting human BAG3, an intrinsically disordered co-chaperone protein critically involved in apoptosis, autophagy, and tumor progression. By integrating orthogonal biophysical methods, including thermal shift assays and ligand-observed NMR spectroscopy, we identified and validated a set of low-molecular-weight fragments capable of binding BAG3. Among these, the 6-chloro-2-oxindole fragment (**Fr1**) emerged as the most promising hit, showing a binding affinity in the high micromolar range and serving as a chemically efficient starting point for hit-to-lead optimization.

Structure–activity relationship (SAR) studies focusing on the 6-chloro-2-oxindole scaffold revealed that hydrophobic substitutions at position 3 enhanced affinity without disrupting the key binding interactions. The optimized analogue, derivative **7**, displayed a significantly improved dissociation constant ($K_D \approx 22$ μM) and successfully displaced the parent fragment in competition NMR experiments, confirming better binding affinity, and the same binding site.

These findings demonstrate the feasibility of targeting BAG3 with small molecules despite its high conformational flexibility and lack of an experimentally resolved structure. Our results provide a validated chemical tool for probing BAG3 function and lay the groundwork for future development of selective BAG3 inhibitors. More broadly, this work highlights the potential of fragment-based strategies to unlock novel therapeutic opportunities for proteins traditionally considered "undruggable," particularly within the class of intrinsically disordered and PPI-mediating proteins. Although the present study focuses on the biophysical identification and optimization of BAG3-binding fragments, further biological validation will be required to assess their functional effects in cellular models.

4. Materials and Methods

4.1. Human BAG3 expression and purification

The *human* BAG3 protein was expressed as a C-terminus His-tagged protein in the *human* HEK-293T cell line as previously reported [14]. Briefly, the pCDNA3.1 C-*ter* His-tagged BAG3 plasmid (namely BAG3-His, Genscript, Piscataway NJ) was transiently transfected into

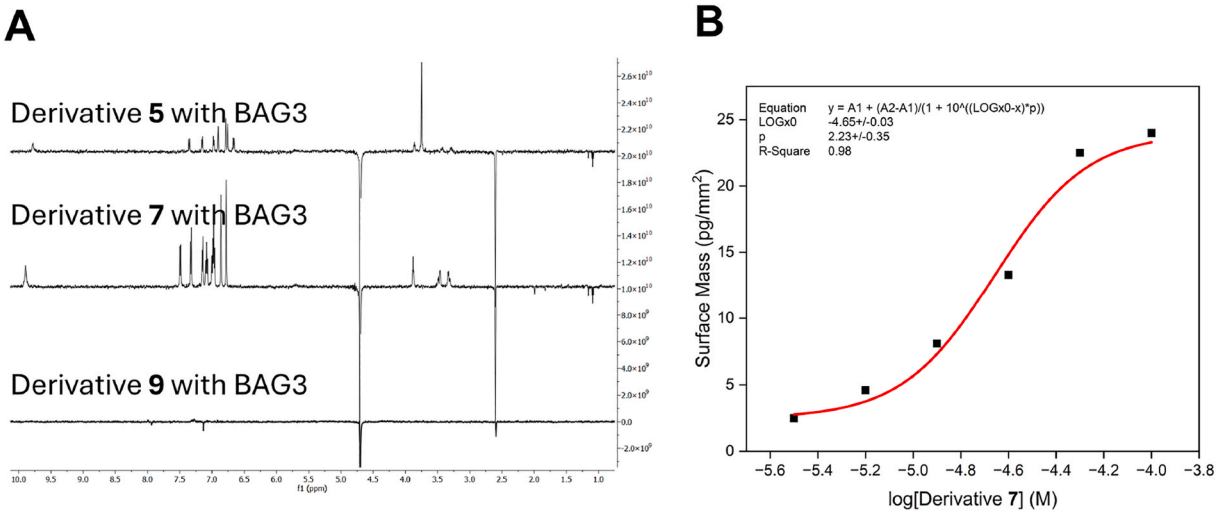

Fig. 4. Biophysical evaluation of three grown molecules selected as *human* BAG3 binders. (**A**) Superposition of WaterLOGSY spectra in the presence of 5 μM *human* BAG3-His of compounds **5**, **7**, and **9** (all at 100 μM), which were selected as *human* BAG3-His binders among the nine 6-chloro-2-oxindole derivatives. Spectra were recorded at 298 K on a 600 MHz spectrometer equipped with a nitrogen-cooled cryoprobe in 50 mM phosphate and 150 mM NaCl at pH 7.8, and are processed, maintaining binders with a positive phase. (**B**) Equilibrium analysis of GCI data for derivative **7.** Surface mass is plotted as a function of log[derivative **7**]. Six concentrations were tested, and a sigmoidal fit (OriginPro) yielded a K_D of around 22 μM, with a Hill slope of 2.23 ± 0.35 ($R^2 = 0.98$). The protein target was injected at 30 μg/mL.

human HEK-293T cells, and after 72 h, the cells were harvested and lysed for protein collection. The cell lysate was clarified by centrifugation (14,000 rpm, 45 min, 4 °C), and the *human* BAG3-His was purified by two subsequent purification steps. A first HisTrap™ column (Cytiva Marlborough, MA, USA) previously equilibrated with 30 mM Tris Buffer, pH 8.3, and 300 mM NaCl, was used to separate the *human* BAG3-His from the total cell proteins. The eluted protein by the imidazole linear gradient (from 15 mM to 500 mM), was further purified by Size Exclusion Chromatography (SEC) on a HiLoad™ 16/60 Superdex™ 200 prep grade column (Cytiva Marlborough, MA, USA), equilibrated with 50 mM sodium phosphate, pH 7.8, 150 mM NaCl, and 0.04% (w/v) NaN_3.

The disorder propensity of the full-length human BAG3 was predicted by using the machine learning-based tool: flDPnn (http://bioinformatics.cs.vcu.edu/servers/flDPnn) [45].

4.2. Fragment library screening

Our fragment library comprises 783 molecules [43], selected based on modern trends in fragment library design. In detail, fragments are characterized by a: molecular weight (MW) between 94 Da and 300 Da (average 187 Da); clogP between −4 and 4 (average 1.4); topological surface area (TPSA) between 0 $Å^2$ and 118 $Å^2$ (average 44 $Å^2$); number of hydrogen bond acceptors between 0 and 6 (average 2); hydrogen bond donors between 0 and 5 (average 1); rotatable bonds between 0 and 10 (average 2) number of heavy atoms (HA) between 7 and 22 (average 13). Fragments exhibit proven solubility in dimethyl sulfoxide (DMSO) at 100 mM and in aqueous solution at 1 mM. Commercially available screening compounds **5**, **6**, **8**, and **9** were purchased from MolPort (ID: MolPort-009-759-084, MolPort-019-156-739, MolPort-018-616-706, MolPort-019-691-834). Molecule structures rendering was prepared with MOE suite [46], Chem Draw 23.1.1 [47], and RDkit Python library. The primary fragment screening was conducted using a thermal shift assay with the ABI PRISM™ 7900HT Fast Real-Time PCR System (Applied Biosystems, Thermo Fisher Scientific, Waltham, MA, USA). Fragments were screened at a final concentration of 2 mM in a total volume of 50 μL, which included *human* BAG3-His (1.5 μM) in assay buffer (50 mM HEPES, pH 7.8), SYPRO Orange™ Protein Gel Stain (Thermo Fisher Scientific, Waltham, MA, USA) (5X final concentration), and one fragment per well. For each plate, three wells containing the protein in assay buffer with 2% (v/v) DMSO were used as blank. The protein was buffer-exchanged into the assay buffer using a HiPrep 26/10 desalting column (Cytiva, Washington, DC, USA) and incubated with one fragment per well. Subsequently, the dye was diluted in ultrapure water and added to each well at a 5X final concentration. The well contents were mixed by centrifugation for 2 min at 500 g before starting the thermal shift experiment. The protocol included an initial equilibration phase (4 °C for 5 min) to allow dye diffusion, followed by heating the plate from 25 to 75 °C in 1 °C increments every 10 s, with fluorescence readings optimized for the dye at 485/20 nm (excitation) and 530/30 nm (emission). Raw data were processed and analyzed by JTSA web-server (Bond, PS. JTSA. http://paulsbond.co.uk/jtsa), with a five-parameter sigmoid equation (Sigmoid-5) selected for curve fitting, and the melting temperature calculated from the midpoint of the curve. Fragments that produced a positive ΔTm of at least 1 °C above the average Tm of the protein were identified as potential *human* BAG3 binders. These fragments were subsequently tested in triplicate under the same conditions, and those that resulted in a positive ΔTm greater than 2 standard deviations (SD) from the Tm, apo were selected as potential *human* BAG3-His hits.

4.3. WaterLOGSY NMR experiments

All the WaterLOGSY experiments were acquired at 298 K on a Bruker 600 MHz spectrometer equipped with an automatic sampler (60 samples) and a nitrogen-cooled cryoprobe, and they were processed and analyzed by Topspin 4.3.1 (Bruker BioSpin GmbH, Rheinstetten, Germany). They were recorded with 256 scans, a recovery delay of 4.5 s before each scan, and a mixing time of 1.7 s. Water suppression was achieved by the excitation sculpting pulse scheme [48]. These experiments were recorded on samples consisting of potential hits from the primary thermal shift screening or the nine 6-chloro-2-oxindoles in the presence and absence of the protein. The NMR samples were prepared in 50 mM sodium phosphate, pH 7.8, 150 mM NaCl, and 0.04% (w/v) NaN_3, and consisted of 100 μM compound in 2% deuterated-DMSO, 5% (v/v) deuterated water, and 5 μM *human* BAG3-His. These experiments enabled a preliminary ranking of validated *human* BAG3-His binders (fragments **Fr1–4** and **Fr6–8**) based on their WaterLOGSY (WLOGSY) factors, calculated for the protons most protected by the protein.

The WLOGSY factor was defined according to the following equation [44]:

$$\mathrm{WLOGSY}_{\mathrm{factor}} = \frac{|I - \mathrm{I}_0|}{|\mathrm{I}_0|} \quad (1)$$

where (I) and (I_0) represent peak intensities in the presence and absence of the protein, respectively. To compare fragments having signals originated from a different number of protons and the WLOSGY factor was normalized by number of protons corresponding to the signal. In the fragment epitope mapping studies, for each fragment the peak with the strongest WLOGSY factors in the spectrum was set to 100% and used as a reference to calculate relative WLOGSY factors of the order fragment signals. To estimate the K_D of **Fr1**, a five-point WaterLOGSY titration was performed using **Fr1** concentrations of 100, 200, 400, 800, and 1000 μM, with a fixed protein concentration of 5 μM. The buffer used was 50 mM sodium phosphate (pH 7.8), 150 mM NaCl, 0.04% (w/v) NaN_3, and 5% (v/v) deuterated water. Deuterated DMSO was maintained at 2% (v/v) in all samples. An additional WaterLOGSY spectrum of the ligand at 1 mM, without protein, was recorded to ensure accurate measurement of the WaterLOGSY effect proportional to ligand concentration. The KD value was determined by averaging the WaterLOGSY effects of protons H1, H2, and H3 (those with the highest WaterLOGSY effects) for each titration point, and plotting these values against ligand concentrations. The data were fitted using Origin 2024b software (OriginLab Corporation, USA) with the following equation [49]:

$$y = \frac{(KD + L0)^{*}x}{(KD + x)^{*}L0} \quad (2)$$

where y, x, and L0 represent the LOGSY effect, the ligand concentration, and the ligand concentration at the first titration point, respectively. The LOGSY effect was normalized (I_norm) to 1 for the ligand concentration L0 and used as a reference to calculate relative LOGSY effects accordingly.

WaterLOGSY competition experiments between **Fr1** and derivative **7** were conducted as follows. First, a WaterLOGSY experiment was performed on a sample containing **Fr1** (100 μM) and the protein (5 μM). Then, derivative **7** was added at a concentration of 100 μM, and another WaterLOGSY experiment was carried out to assess displacement activity. Control samples without protein were also prepared. The buffer used consisted of 50 mM sodium phosphate (pH 7.8) 150 mM NaCl, and 5% (v/v) deuterated water. The concentration of d6-DMSO was kept at 2% (v/v) in all samples.

4.4. Grating-coupled interferometry

GCI binding experiments were carried out using a Creoptix WAVEsystem (Creoptix AG, Switzerland) equipped with a 4PCH sensor chip (polycarboxylate hydrogel surface) at 25 °C. The sensor surface was activated using a freshly prepared mixture of 100 μM N-ethyl-N′-(3-dimethylaminopropyl)carbodiimide (EDC) and 100 μM N-hydroxysuccinimide (NHS), followed by immobilization of *human* BAG3-His protein injected at 30 μg/mL in 10 mM sodium acetate buffer at pH 4.2. The injection was repeated three times to achieve the desired

immobilization level. After coupling, the surface was quenched with 1 M ethanolamine (pH 8.0) and conditioned with borate buffer as per the manufacturer's protocol. A reference channel underwent the same activation and deactivation procedures in the absence of protein and was used for background subtraction. Compound **7** was tested in a six-point 1:2 serial dilution starting from 100 μM, prepared in PBS containing 3% DMSO. Each concentration was injected at 400 μL/min for 60 s (association phase), followed by a 120 s dissociation phase under continuous flow of running buffer. A DMSO calibration curve was recorded and applied to correct for bulk refractive index effects. Sensorgrams were processed using WAVEcontrol software (Creoptix AG). Kinetic fitting was first performed using the instrument's integrated tools, and equilibrium responses were extracted at steady state. The apparent equilibrium dissociation constant (K_D) was determined by nonlinear regression of the equilibrium binding signal as a function of compound concentration using a sigmoidal dose–response model in OriginPro (OriginLab).

4.5. Chemistry

^{1}H and ^{13}C NMR spectra were recorded on a Varian 400 Mercury Plus spectrometer (Palo Alto, CA, USA). Chemical shifts (δ) are given in ppm upfield, and the spectra were recorded in appropriate deuterated solvents, as indicated. Mass spectra were recorded by an ESI single quadrupole mass spectrometer (Waters ZQ 2000; Waters Instruments, UK), and the values are expressed as $[M+1]^+$. Melting points (mp) were determined on a Buchi-Tottoli apparatus and are uncorrected. All products reported showed ^{1}H and ^{13}C NMR spectra in agreement with the assigned structures. The purity of tested compounds was determined by combustion elemental analyses conducted by the Microanalytical Laboratory of the Chemistry Department of the University of Ferrara with a Yanagimoto MT-5 CHN recording elemental analyzer. All tested compounds yielded data consistent with a purity of at least 95% as compared with the theoretical values. Reaction courses and product mixtures were routinely monitored by TLC on silica gel (precoated F254 Merck plates), and compounds were visualized with aqueous $KMnO_4$. Flash chromatography was performed using 230-400 mesh silica gel and the indicated solvent system. Organic solutions were dried over anhydrous Na_2SO_4.

4.5.1. General procedure for the preparation of derivatives 2—4

To a solution of 6-chloroisatin (310 mg, 1.71 mmol) in dry DMF (3 mL), sodium hydride (as a 60% dispersion in mineral oil; 75 mg, 1.88 mmol, 1.1 equiv.) was added under N_2 atmosphere at 0 °C, and the resulting reaction mixture was maintained in an ice bath for 10 min. The reaction mixture was allowed to reach room temperature and stirred for 30 min, after which the appropriate bromoalkyl ester (1.88 mmol, 1.1 equiv.) was added dropwise. After stirring overnight, the reaction mixture was quenched with saturated NH_4Cl solution, diluted with water and extracted with EtOAc (2X). The combined organic phases were washed with a saturated NaCl solution, dried over anhydrous Na_2SO_4, filtered, and concentrated under reduced pressure. The crude residue was purified by silica gel flash chromatography using ethyl acetate and petroleum ether as the eluent system, yielding derivatives **2**–**4**.

(+/−)-Ethyl 2-(6-chloro-2,3-dioxoindolin-1-yl)propanoate (derivative **2**). Following general procedure, using 2-bromopropanoic acid ethyl ester (0.21 mL, 1.88 mmol) as alkylating agent, the crude product was purified by flash column chromatography by using petroleum ether-ethyl acetate 8-2 as eluent to give derivative 2 as an orange solid. Yield: 62%, mp 118-119 °C. ^{1}H NMR (400 MHz, d_6-DMSO) δ: 1.16 (t, J = 7.1 Hz, 3H), 1.56 (d, J = 7.2 Hz, 3H), 4.15 (d, J = 7.1 Hz, 2H), 5.14 (q, J = 7.2 Hz, 1H), 7.23 (dd, J = 8.0 and 1.7 Hz, 1H), 7.38 (d, J = 1.7 Hz, 1H), 7.63 (d, J = 8.0 Hz, 1H). ^{13}C NMR (101 MHz, d_6-DMSO) δ: 14.44, 41.84, 61.87, 112,21, 116.64, 124.02, 126.59, 143,26, 152,02, 158.70, 167.79, 181.66, MS (ESI) *m/z* calculated for $C_{13}H_{12}ClNO_4$ $[M+1]^+$ = 281.05, found 282.11 and 284.24.

Ethyl 3-(6-chloro-2,3-dioxoindolin-1-yl)propanoate (derivative **3**). Following general procedure, using ethyl 3-bromopropanoate (0.23 mL, 1.88 mmol) as alkylating agent, the crude product was purified by flash column chromatography by using petroleum ether-ethyl acetate 8-2 as eluent to give derivative 3 as an orange solid. Yield: 71%, mp 124-126 °C. ^{1}H NMR (400 MHz, d_6-DMSO) δ: 1.18 (t, J = 7.0 Hz, 3H), 2.93 (t, J = 8.0 Hz, 2H), 3.59 (t, J = 8.0 Hz, 2H), 4.06 (q, J = 7.2 Hz, 2H), 6.91 (dd, J = 8.0 and 1.7 Hz, 1H), 7.07 (d, J = 1.7 Hz, 1H), 7.49 (d, J = 8.0 Hz, 1H). ^{13}C NMR (101 MHz, d_6-DMSO) δ: 14.52, 28.51, 37.62, 60.76, 112.61, 117.18, 123.13, 126.64, 142.74, 152,26, 159.83, 170.69, 183.40. MS (ESI) *m/z* calculated for $C_{13}H_{12}ClNO_4$ $[M+1]^+$ = 281.05, found found 282.12 and 284.22.

Ethyl 2-(6-chloro-2,3-dioxoindolin-1-yl)acetate (derivative **4**). Following general procedure, using ethyl bromoacetate (0.21 mL, 1.88 mmol) as alkylating agent, the crude product was purified by flash column chromatography by using petroleum ether-ethyl acetate 8-2 as eluent to give derivative 4 as a yellow solid. Yield: 63%, mp 118-120 °C. ^{1}H NMR (400 MHz, DMSO-d_6) δ: 1.22 (t, J = 7.1 Hz, 3H), 4.17 (q, J = 7.1 Hz, 2H), 4.62 (s, 2H), 7.22 (dd, J = 8.0 and 1.7 Hz, 1H), 7.47 (d, J = 1.7 Hz, 1H), 7.63 (d, J = 8.0 Hz, 1H). ^{13}C NMR (101 MHz, d_6-DMSO) δ: 14.40, 39.97, 49.93, 61.85, 112.02, 116.97, 123.81, 126.75, 143.12, 151.47, 158.23, 169.64, 181.72. MS (ESI) *m/z* calculated for $C_{13}H_{12}ClNO_4$ $[M+1]^+$ = 267.03, found 268.23 and 270.17.

4.5.1.1. Preparation of (Z)-3-((1H-indol-3-yl)methylene)-6-chloroindolin-2-one. A solution of 6-chlorooxindole (168 mg, 1.0 mmol), indole-3-carboxaldehyde (145 mg, 1.0 mmol, 1 equiv.) and piperidine (11 μL, 01 mmol, 0.1 equiv) in ethanol (10 mL) was heated to reflux for 4 h. After completion of the reaction, the solvent was removed under reduced pressure. The resulting solid residue was suspended in ethyl ether (10 mL), and the mixture was cooled in an ice bath. The precipitate was filtered, washed with ethyl ether to furnish the target compound as a yellow solid. Yield: 68%, mp 184-186 °C. ^{1}H NMR (400 MHz, d_6-DMSO) δ: 6.71 (d, J = 8.0 Hz, 1H), 6.88 (d, J = 2.0 Hz, 1H), 6.96 (dd, J = 8.0 and 1.8 Hz, 1H), 7.21 (t, J = 7.5 Hz, 1H), 7.43 (t, J = 7.6 Hz, 1H), 7.90 (d, J = 8.1 Hz, 1H), 8.17 (d, J = 7.9 Hz, 1H), 8.21 (d, J = 1.8 Hz, 1H), 9.45 (s, 1H), 10.6 (s, 1H), 12.6 (s, 1H). MS (ESI): $[M+1]^+$ = 295.07 and 297.07.

4.5.1.2. Preparation of (+/−)-3-(1H-indol-3-yl)methyl)-6-chloroindolin-2-one (derivative 7). $NaBH_4$ (95 mg, 2.5 mmol, 5 equiv.) was added to an ice-cooled reaction mixture of (Z)-3-((1*H*-indol-3-yl)methylene)-6-chloroindolin-2-one (147 mg, 0.5 mmol) in ethanol (5 mL). After that, the reaction mixture was warmed to room temperature and stirred for 4 h. The reaction was quenched with a saturated aqueous solution of NH_4Cl, diluted with 1 M hydrochloric acid (5 mL), and extracted with EtOAc (3x), washed with brine, dried over anhydrous Na_2SO_4, evaporated and the residue was purified by column chromatography by using petroleum ether-ethyl acetate 1-1 as eluent to give derivative 7 as a yellow solid. Yield: 73%, mp 176-178 °C. ^{1}H NMR (400 MHz, d_6-DMSO) δ: 3.08 (dd, J = 14.5 and 4.5 Hz, 1H), 3.36 (dd, J = 8.9 and 4.5 Hz, 1H), 3.76 (dd, J = 8.9 and 4.5 Hz, 1H), 6.68 (d, J = 2.0 Hz, 1H), 6.83 (dd, J = 8.0 and 2.0 Hz, 1H), 6.91 (m, 2H), 6.96 (d, J = 7.6 Hz, 1H), 6.99 (t, J = 8.1 Hz, 1H), 7.26 (d, J = 7.6 Hz, 1H), 7.50 (d, J = 7.6 Hz, 1H), 10.4 (s, 1H), 10.7 (s, 1H). ^{13}C NMR (101 MHz, d_6-DMSO) δ 179.08, 144.78, 136.33, 132.15, 129.16, 127.62, 126.13, 123.97, 121.32, 120.97, 118.95, 118.72, 111.72, 110.60, 109.44, 46.14, 25.54. MS (ESI): $[M+1]^+$ = 297.13 and 299.12.

CRediT authorship contribution statement

Annagiulia Favaro: Writing – original draft, Investigation, Data curation. **Chiara Marchioro:** Investigation. **Martina Canton:** Investigation. **Thomas Stella:** Investigation, Data curation. **Romeo Romagnoli:** Investigation, Data curation. **Elena Mariotto:** Writing – review & editing, Supervision, Data curation, Conceptualization. **Mattia**

Sturlese: Writing – review & editing, Investigation, Data curation, Conceptualization. **Giampietro Viola:** Writing – review & editing, Supervision, Funding acquisition, Conceptualization.

Declaration of competing interest

The authors declare that they have no known competing financial interests or personal relationships that could have appeared to influence the work reported in this paper.

Aknowledgment

The research leading to these results has received funding from AIRC under IG 2019 - ID 23109 project (GV). The financial support of UNIPD@STARS-StG (#STUMBLE) and IRP-StG 2023 (#24/12 IRP), as well as individual fellowship from AIRC (ID 24185) and from Umberto Veronesi Foundation (FUV #5318) to E.M. M.C was supported by Fondazione Città della Speranza PhD Scholarship. We are grateful to Dr. Andrea Bertarello of the Screening Facility of the Department of Pharmaceutical and Pharmacological Sciences of the University of Padova (SF@DSF) for the support with the GCI experiments.

Appendix A. Supplementary data

Supplementary data to this article can be found online at https://doi.org/10.1016/j.ejmcr.2026.100327.

Data availability

Data will be made available on request.

References

[1] S. Takayama, et al., Cloning and functional analysis of BAG-1: a novel Bcl-2-binding protein with anti-cell death activity, Cell. 80 (2) (Jan. 1995) 279–284, https://doi.org/10.1016/0092-8674(95)90410-7.
[2] S. Takayama, et al., BAG-1 modulates the chaperone activity of Hsp70/Hsc70, EMBO J. 16 (16) (Aug. 1997) 4887–4896, https://doi.org/10.1093/emboj/16.16.4887.
[3] S. Takayama, Z. Xie, J.C. Reed, An evolutionarily conserved family of Hsp70/Hsc70 molecular chaperone regulators, J. Biol. Chem. 274 (2) (Jan. 1999) 781–786, https://doi.org/10.1074/jbc.274.2.781.
[4] H.-Q. Wang, et al., Characterization of BAG3 cleavage during apoptosis of pancreatic cancer cells, J. Cell. Physiol. 224 (1) (Jul. 2010) 94–100, https://doi.org/10.1002/jcp.22097.
[5] H. Doong, K. Rizzo, S. Fang, V. Kulpa, A.M. Weissman, E.C. Kohn, CAIR-1/BAG-3 abrogates heat shock protein-70 chaperone complex-mediated protein degradation: accumulation of poly-ubiquitinated Hsp90 client proteins, J. Biol. Chem. 278 (31) (Aug. 2003) 28490–28500, https://doi.org/10.1074/jbc.M209682200.
[6] Z.-X. Du, X. Meng, H.-Y. Zhang, Y. Guan, H.-Q. Wang, Caspase-dependent cleavage of BAG3 in proteasome inhibitors-induced apoptosis in thyroid cancer cells, Biochem. Biophys. Res. Commun. 369 (3) (May 2008) 894–898, https://doi.org/10.1016/j.bbrc.2008.02.112.
[7] P. Liu, B. Xu, J. Li, H. Lu, BAG3 gene silencing sensitizes leukemic cells to Bortezomib-induced apoptosis, FEBS Lett. 583 (2) (Jan. 2009) 401–406, https://doi.org/10.1016/j.febslet.2008.12.032.
[8] M. Festa, et al., BAG3 protein is overexpressed in human glioblastoma and is a potential target for therapy, Am. J. Pathol. 178 (6) (Jun. 2011) 2504–2512, https://doi.org/10.1016/j.ajpath.2011.02.002.
[9] H. Doong, A. Vrailas, E.C. Kohn, What's in the 'BAG'?–A functional domain analysis of the BAG-family proteins, Cancer Lett. 188 (1–2) (Dec. 2002) 25–32, https://doi.org/10.1016/S0304-3835(02)00456-1.
[10] A. Rosati, V. Graziano, V. De Laurenzi, M. Pascale, M.C. Turco, BAG3: a multifaceted protein that regulates major cell pathways, Cell Death Dis. 2 (4) (Apr. 2011) e141, https://doi.org/10.1038/cddis.2011.24.
[11] V. Arndt, et al., Chaperone-assisted selective autophagy is essential for muscle maintenance, Curr. Biol. 20 (2) (Jan. 2010) 143–148, https://doi.org/10.1016/j.cub.2009.11.022.
[12] C. Behl, BAG3 and friends: co-chaperones in selective autophagy during aging and disease, Autophagy 7 (7) (Jul. 2011) 795–798, https://doi.org/10.4161/auto.7.7.15844.
[13] M. De Marco, M.C. Turco, L. Marzullo, BAG3 in tumor resistance to therapy, Trends Cancer. 6 (12) (Dec. 2020) 985–988, https://doi.org/10.1016/j.trecan.2020.07.001.
[14] F. Budassi, et al., Design, synthesis and biological evaluation of novel 2,4-thiazolidinedione derivatives able to target the human BAG3 protein, Eur. J. Med. Chem. 261 (Dec. 2023) 115824, https://doi.org/10.1016/j.ejmech.2023.115824.
[15] E. Stürner, C. Behl, The role of the multifunctional BAG3 protein in cellular protein quality control and in disease, Front. Mol. Neurosci. 10 (Jun. 2017) 177, https://doi.org/10.3389/fnmol.2017.00177.
[16] C.M. Brenner, et al., BAG3: nature's quintessential multi-functional protein functions as a ubiquitous intra-cellular glue, Cells. 12 (6) (Mar. 2023), https://doi.org/10.3390/cells12060937.
[17] E. Mariotto, G. Viola, C. Zanon, S. Aveic, A BAG's life: every connection matters in cancer, Pharmacol. Ther. 209 (May 2020) 107498, https://doi.org/10.1016/j.pharmthera.2020.107498.
[18] C. Behl, Breaking BAG: the Co-Chaperone BAG3 in health and disease, Trends Pharmacol. Sci. 37 (8) (Aug. 2016) 672–688, https://doi.org/10.1016/j.tips.2016.04.007.
[19] D. Kögel, B. Linder, A. Brunschweiger, S. Chines, C. Behl, At the crossroads of apoptosis and autophagy: multiple roles of the Co-Chaperone BAG3 in stress and therapy resistance of cancer, Cells. 9 (3) (Feb. 2020), https://doi.org/10.3390/cells9030574.
[20] A. Rosati, et al., Apoptosis inhibition in cancer cells: a novel molecular pathway that involves BAG3 protein, Int. J. Biochem. Cell Biol. 39 (7–8) (Mar. 2007) 1337–1342, https://doi.org/10.1016/j.biocel.2007.03.007.
[21] G. Chiappetta, et al., The antiapoptotic protein BAG3 is expressed in thyroid carcinomas and modulates apoptosis mediated by tumor necrosis factor-related apoptosis-inducing ligand, J. Clin. Endocrinol. Metab. 92 (3) (Mar. 2007) 1159–1163, https://doi.org/10.1210/jc.2006-1712.
[22] N. Li, et al., PKCδ-mediated phosphorylation of BAG3 at Ser187 site induces epithelial-mesenchymal transition and enhances invasiveness in thyroid cancer FRO cells, Oncogene. 32 (38) (Sep. 2013) 4539–4548, https://doi.org/10.1038/onc.2012.466.
[23] R.D. Finn, et al., Pfam: the protein families database, Nucleic Acids Res. 42 (Database issue) (Jan. 2014) D222–D230, https://doi.org/10.1093/nar/gkt1223.
[24] Y. Chen, et al., Bcl2-associated athanogene 3 interactome analysis reveals a new role in modulating proteasome activity, Mol. Cell. Proteomics 12 (10) (Oct. 2013) 2804–2819, https://doi.org/10.1074/mcp.M112.025882.
[25] L. Marzullo, M.C. Turco, M. De Marco, The multiple activities of BAG3 protein: mechanisms, Biochim. Biophys. Acta Gen. Subj. 1864 (8) (Aug. 2020) 129628, https://doi.org/10.1016/j.bbagen.2020.129628.
[26] S. Carra, S.J. Seguin, H. Lambert, J. Landry, HspB8 chaperone activity toward poly (Q)-containing proteins depends on its association with Bag3, a stimulator of macroautophagy, J. Biol. Chem. 283 (3) (Jan. 2008) 1437–1444, https://doi.org/10.1074/jbc.M706304200.
[27] M. Gamerdinger, A.M. Kaya, U. Wolfrum, A.M. Clement, C. Behl, BAG3 mediates chaperone-based aggresome-targeting and selective autophagy of misfolded proteins, EMBO Rep. 12 (2) (Feb. 2011) 149–156, https://doi.org/10.1038/embor.2010.203.
[28] Z. Xu, et al., 14-3-3 protein targets misfolded chaperone-associated proteins to aggresomes, J. Cell Sci. 126 (Pt 18) (Sep. 2013) 4173–4186, https://doi.org/10.1242/jcs.126102.
[29] A. Arakawa, et al., The C-terminal BAG domain of BAG5 induces conformational changes of the Hsp70 nucleotide-binding domain for ADP-ATP exchange, Structure. 18 (3) (Mar. 2010) 309–319, https://doi.org/10.1016/j.str.2010.01.004.
[30] S. Fang, L. Li, B. Cui, S. Men, Y. Shen, X. Yang, Structural insight into plant programmed cell death mediated by BAG proteins in Arabidopsis thaliana, Acta Crystallogr. D Biol. Crystallogr. 69 (Pt 6) (Jun. 2013) 934–945, https://doi.org/10.1107/S0907444913003624.
[31] K. Koya, et al., MKT-077, a novel rhodacyanine dye in clinical trials, exhibits anticarcinoma activity in preclinical studies based on selective mitochondrial accumulation, Cancer Res. 56 (3) (Feb. 1996) 538–543.
[32] Y. Miyata, et al., Synthesis and initial evaluation of YM-08, a blood-brain barrier permeable derivative of the heat shock protein 70 (Hsp70) inhibitor MKT-077, which reduces tau levels, ACS Chem. Neurosci. 4 (6) (Jun. 2013) 930–939, https://doi.org/10.1021/cn300210g.
[33] X. Li, et al., Validation of the Hsp70-Bag3 protein-protein interaction as a potential therapeutic target in cancer, Mol. Cancer Therapeut. 14 (3) (Mar. 2015) 642–648, https://doi.org/10.1158/1535-7163.MCT-14-0650.
[34] S. Terracciano, et al., Discovery and synthesis of the first selective BAG domain modulator of BAG3 as an attractive candidate for the development of a new class of chemotherapeutics, Chem. Commun. 54 (55) (Jul. 2018) 7613–7616, https://doi.org/10.1039/c8cc03399d.
[35] D. Ruggiero, et al., Structural refinement of 2,4-Thiazolidinedione derivatives as new anticancer agents able to modulate the BAG3 protein, Molecules 27 (3) (Jan. 2022), https://doi.org/10.3390/molecules27030665.
[36] D.A. Erlanson, B.J. Davis, W. Jahnke, Fragment-based drug discovery: advancing fragments in the absence of crystal structures, Cell Chem. Biol. 26 (1) (Jan. 2019) 9–15, https://doi.org/10.1016/j.chembiol.2018.10.001.
[37] Q. Li, Application of fragment-based drug discovery to versatile targets, Front. Mol. Biosci. 7 (Aug. 2020) 180, https://doi.org/10.3389/fmolb.2020.00180.
[38] M.M. Hann, A.R. Leach, G. Harper, Molecular complexity and its impact on the probability of finding leads for drug discovery, J. Chem. Inf. Comput. Sci. 41 (3) (2001) 856–864, https://doi.org/10.1021/ci000403i.
[39] R.J. Hall, P.N. Mortenson, C.W. Murray, Efficient exploration of chemical space by fragment-based screening, Prog. Biophys. Mol. Biol. 116 (2–3) (Sep. 2014) 82–91, https://doi.org/10.1016/j.pbiomolbio.2014.09.007.

[40] J.A. Wells, C.L. McClendon, Reaching for high-hanging fruit in drug discovery at protein-protein interfaces, Nature. 450 (7172) (Dec. 2007) 1001–1009, https://doi.org/10.1038/nature06526.
[41] A.A. Bogan, K.S. Thorn, Anatomy of hot spots in protein interfaces, J. Mol. Biol. 280 (1) (Jul. 1998) 1–9, https://doi.org/10.1006/jmbi.1998.1843.
[42] A.J. Price, S. Howard, B.D. Cons, Fragment-based drug discovery and its application to challenging drug targets, Essays Biochem. 61 (5) (Nov. 2017) 475–484, https://doi.org/10.1042/EBC20170029.
[43] A. Favaro, G. Bolcato, M.A. Comini, S. Moro, M. Bellanda, M. Sturlese, Drugging the undruggable Trypanosoma brucei monothiol glutaredoxin 1, Molecules 28 (3) (Jan. 2023), https://doi.org/10.3390/molecules28031276.
[44] C. Raingeval, O. Cala, B. Brion, M. Le Borgne, R.E. Hubbard, I. Krimm, 1D NMR WaterLOGSY as an efficient method for fragment-based lead discovery, J. Enzym. Inhib. Med. Chem. 34 (1) (Dec. 2019) 1218–1225, https://doi.org/10.1080/14756366.2019.1636235.
[45] G. Hu, et al., flDPnn: accurate intrinsic disorder prediction with putative propensities of disorder functions, Nat. Commun. 12 (1) (Jul. 2021) 4438, https://doi.org/10.1038/s41467-021-24773-7.
[46] Chemical Computing Group, *MOE (Molecular Operating Environment)*, Chemical Computing Group (2020). Montreal, QC, Canada.
[47] PerkinElmer Informatics, *ChemDraw*, Perkinelmer Informatics, 2024.
[48] T.L. Hwang, A.J. Shaka, Water suppression that works. Excitation sculpting using arbitrary wave-forms and pulsed-field gradients, J. Magn. Reson., Ser. A 112 (2) (Feb. 1995) 275–279, https://doi.org/10.1006/jmra.1995.1047.
[49] C. Dalvit, A. Parent, F. Vallée, M. Mathieu, A. Rak, Fast NMR methods for measuring in the direct and/or competition mode the dissociation constants of chemical fragments interacting with a receptor, ChemMedChem. 14 (11) (Jun. 2019) 1115–1127, https://doi.org/10.1002/cmdc.201900152.